Therapeutic Applications of Spherical Nucleic Acids

Stacey N. Barnaby, Timothy L. Sita, Sarah Hurst Petrosko, Alexander H. Stegh and Chad A. Mirkin

Abstract

Spherical nucleic acids (SNAs) represent an emerging class of nanoparticle-based therapeutics. SNAs consist of densely functionalized and highly oriented oligonucleotides on the surface of a nanoparticle which can either be inorganic (such as gold or platinum) or hollow (such as liposomal or silica-based). The spherical architecture of the oligonucleotide shell confers unique advantages over traditional nucleic acid delivery methods, including entry into nearly all cells independent of transfection agents and resistance to nuclease degradation. Furthermore, SNAs can penetrate biological barriers, including the blood–brain and blood–tumor barriers as well as the epidermis, and have demonstrated

Stacey N. Barnaby and Timothy L. Sita contributed equally to this work.

S.N. Barnaby · S.H. Petrosko · C.A. Mirkin (✉)
Department of Chemistry, Northwestern University,
2145 Sheridan Road, Evanston, IL 60208, USA
e-mail: chadnano@northwestern.edu

S.N. Barnaby · T.L. Sita · S.H. Petrosko · A.H. Stegh (✉) · C.A. Mirkin
International Institute for Nanotechnology, Northwestern University,
2145 Sheridan Road, Evanston, IL 60208, USA
e-mail: a-stegh@northwestern.edu

T.L. Sita · C.A. Mirkin
Interdepartmental Biological Sciences Program, Northwestern University,
2205 Tech Drive, Evanston, IL 60208, USA

A.H. Stegh
Ken and Ruth Davee Department of Neurology, The Northwestern Brain Tumor Institute,
the Robert H. Lurie Comprehensive Cancer Center, Northwestern University,
303 East Superior, Chicago, IL 60611, USA

C.A. Mirkin et al. (eds.), *Nanotechnology-Based Precision Tools for the Detection and Treatment of Cancer*, Cancer Treatment and Research 166,
DOI 10.1007/978-3-319-16555-4_2

efficacy in several murine disease models in the absence of significant adverse side effects. In this chapter, we will focus on the applications of SNAs in cancer therapy as well as discuss multimodal SNAs for drug delivery and imaging.

Keywords
Spherical nucleic acids · SNAs · siRNA · Nanoparticles · Cancer · Therapeutics

Contents

1 Introduction

Nucleic acid-based therapeutic agents typically consist of short strands of oligonucleotides that are capable of performing gene regulatory functions. The DNA and RNA comprising such therapeutics can be customized to selectively silence any mutated or deregulated genes, thus offering tremendous potential as tools for precision medicine, where patient-specific treatments are designed to address the genetic basis underlying an individual patient's disease [1, 2].

Nucleic acid-based therapeutics can be primarily divided into two categories: those that are comprised of double-stranded RNA (dsRNA) molecules that function via the RNA interference (RNAi) pathway and those that consist of single-stranded DNA molecules that act as antisense oligonucleotides (ASO). Both types can interfere with mRNA molecules to silence protein expression, and many of these structures have been extensively investigated in clinical trials for cancer, hereditary disorders, heart disease, inflammatory conditions, and viral infections [3–6]. The mechanisms of action of these two types of oligonucleotide-based therapeutics differ as described briefly below (for additional information see [7] (for RNAi-based gene silencing) and [8] (for ASO-based silencing)).

1.1 Antisense Oligonucleotides (ASOs)

ASOs can inhibit protein translation via either a steric blockade of translation or the recruitment of the endonuclease RNase H [8, 9]. The former method involves sequence-specific binding of ASOs to target mRNA in the cytoplasm, thereby preventing ribosomal translation of the mRNA (Fig. 1a). The latter mechanism involves RNase H-dependent cleavage, in which RNase H recognizes an RNA–DNA heteroduplex, selectively cleaves the RNA strand, and releases the intact DNA strand [10]. The intact DNA strand can then engage additional target mRNAs and recruit RNase H, enhancing its potency.

1.2 The RNA Interference (RNAi) Pathway

Fire and Mello first reported the discovery of RNAi-based gene silencing in *Caenorhabditis elegans* in 1998. This discovery later earned them the Nobel Prize in Physiology or Medicine in 2006 [11]. The RNAi pathway was then established in mammalian cells by Tuschl and colleagues, prompting rigorous development of RNAi-based therapeutics to battle diseases previously considered "undruggable" by traditional pharmaceutical approaches (i.e., small molecules and biotherapeutic antibodies) [12–15]. The RNAi pathway is activated by the presence of dsRNA in the cytoplasm (Fig. 1b) [16–18]. Dicer, a cytoplasmic endoribonuclease, cleaves longer dsRNA into small interfering RNA (siRNA) or microRNA (miRNA) segments, which are typically 21–23 nucleotides in length. The "antisense" or "guide" strands of siRNA or miRNA segments are then recognized and loaded into the RNA-induced

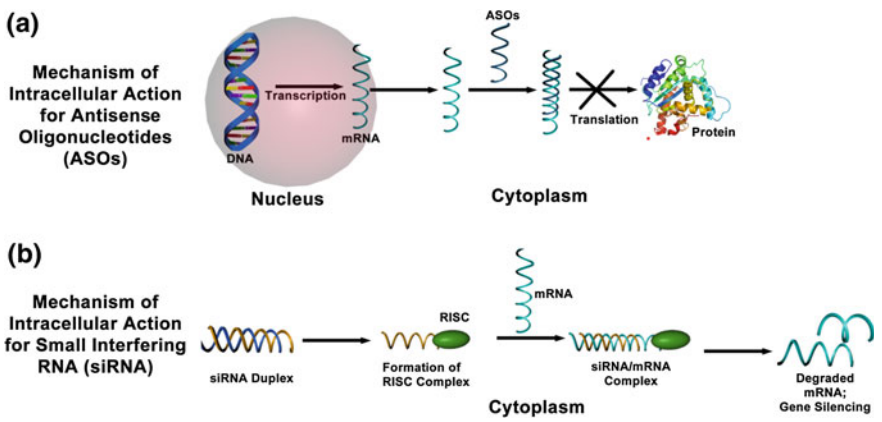

Fig. 1 Different mechanisms of intracellular action of antisense oligonucleotides (ASOs) and small interfering RNAs (siRNAs). **a** Mechanism of action for ASOs, which bind complementary mRNA and cause inhibition of translation or recruit RNase H to cleave the RNA moiety within an RNA–DNA duplex; **b** Mechanism of action for siRNAs, which includes formation of the RNA-induced silencing complex (RISC) and subsequent degradation of target mRNA

silencing complex (RISC), while the "sense" or "passenger strands" are degraded. This activates the RISC complex, leading to Watson-Crick base pairing of complementary target mRNA. Once the target mRNA is bound, its expression can be modified by distinct mechanisms, depending on the biological context. In siRNA-based RNAi, Argonaute 2 (Ago2, an RNA endonuclease in the RISC complex) subsequently cleaves the target mRNA, thereby inhibiting its translation. The RISC complex is recycled and thus cleaves mRNA continuously, resulting in persistent knockdown lasting between 3 and 7 days in dividing cells and up to 3–4 weeks in nondividing cells [19]. In miRNA-based RNAi, multiple mechanisms of silencing are possible, including repression of protein translation and/or deadenylation of target mRNA subsequently leading to its degradation [7, 20].

1.3 Challenges for Oligonucleotide Drug Delivery

Despite these cellular mechanisms that allow for highly specific therapeutic manipulation of genetic expression, a number of barriers to effective delivery are encountered when nucleic acids are systemically injected, limiting their utility in vivo. Unmodified oligonucleotides experience rapid renal clearance, are subject to cleavage by RNases and DNases in serum, and display inefficient uptake by target tissues. Additionally, unmodified oligonucleotides do not efficiently cross the cell membranes and have been shown to trigger a cellular immune response [21–23]. These in vivo barriers to oligonucleotide delivery have slowed the translation of nucleic acid-based therapeutics to the clinic and mandated the use of oligonucleotide-carrier systems, such as polymers/polyplexes [24, 25], dendrimers [26], and lipids [27, 28]. Notably, each of these systems has their own safety concerns and delivery limitations [29]. Nanomaterial-based systems have emerged as potential therapeutic agents for delivering oligonucleotides to cells, and early experiments have shown their great promise [30–32]. Among nanomaterials, spherical nucleic acids (SNAs; Fig. 2) represent an attractive class of single-entity agents, where therapeutic oligonucleotides that can be designed and synthesized to function through either the RNAi or antisense pathway; and these structures are the focus of this chapter.

1.4 Spherical Nucleic Acids (SNAs)

SNAs, typically composed of densely functionalized and highly oriented nucleic acids on nanoparticle cores, represent an emerging class of therapeutics for diseases, including many forms of cancer, because they are capable of overcoming the limitations of traditional oligonucleotide delivery methods and provide an alternative path to gene regulation (Fig. 3) [33, 34]. SNAs are single-entity agents that exhibit unique chemical and physical properties in biological environments. They are readily taken up by almost any type of cell (over 60 tested to date) in high quantities without the use of ancillary transfection reagents ($>10^6$ nanoparticles per

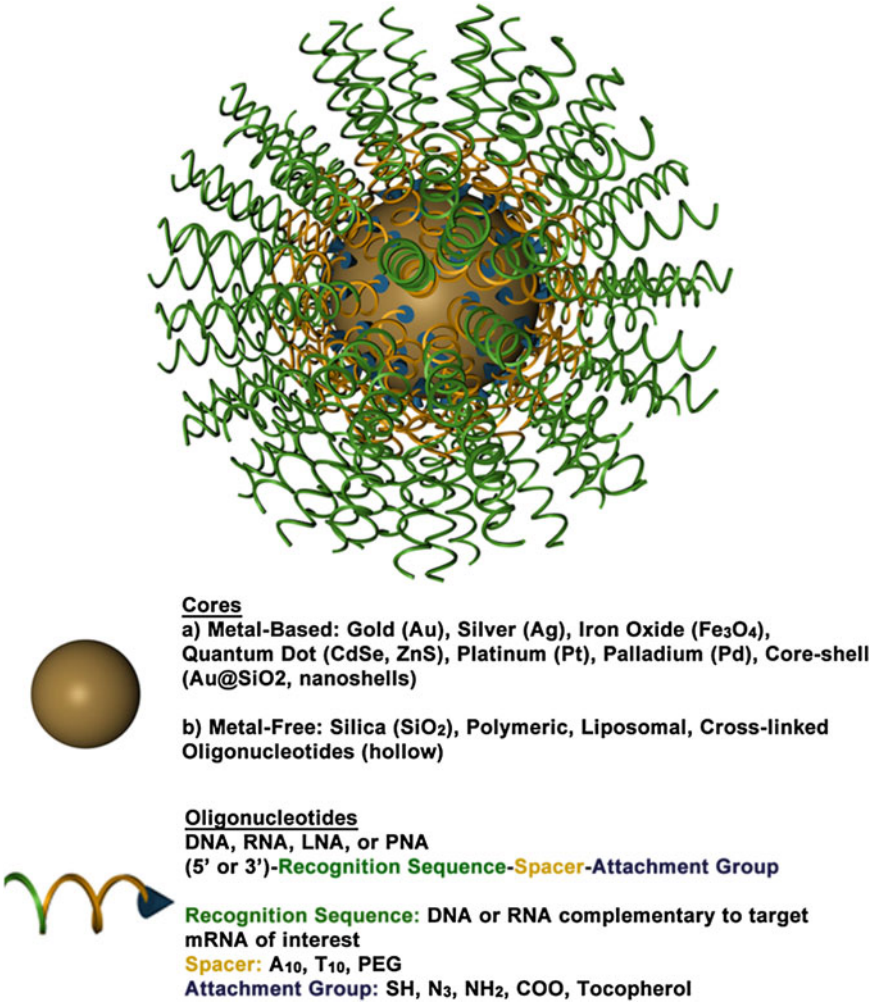

Fig. 2 A 3D drawing of a spherical nucleic acid (SNA). SNAs consist of densely functionalized and highly oriented nucleic acids on the surface of a nanoparticle. Because the properties of SNAs are derived from the shell of nucleic acids, many different cores can be used, such as metal nanoparticles (Au, Pt, etc.), liposomes, and polymers. SNAs can even be core-free. Adapted with permission from Cutler et al. [33]. Copyright 2012. American Chemical Society

cell) [35] through caveolae-mediated endocytosis initiated by recognition through class A scavenger receptors (SR-A) [36, 37]. They elicit a minimal immune response (i.e., 25-fold reduced immune response compared to delivery by cationic carriers) [38, 39] and exhibit increased stability compared to free oligonucleotides in solution [40–43]. These properties stem from the dense shell of highly oriented nucleic acids presented at the surface of these structures [33, 44, 45]. The fact that SNAs facilely enter cells without causing a significant immune response makes

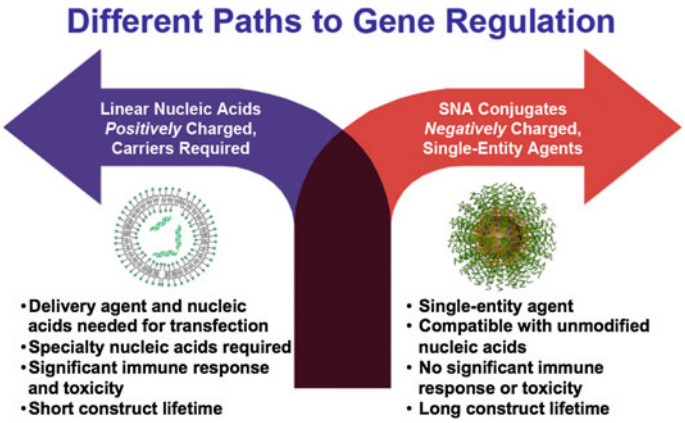

Fig. 3 SNAs offer a different paradigm for gene regulation, where negatively charged nucleic acids do not need to be precomplexed with synthetic positively charged carriers to enter cells and cause gene regulation. If the nucleic acids are densely oriented at the nanoscale, they enter cells in high numbers, exhibit nuclease resistance, show no apparent toxicity, and do not activate the innate immune response. Reproduced with permission from Cutler et al. [33]. Copyright 2012. American Chemical Society

them ideal for local delivery, such as through the skin; however, the fact that they are nonspecifically picked up by nearly all cells will need to be addressed for systemic applications.

The composition of SNAs is highly tailorable, making them an ideal therapeutic platform because they can be tuned to meet the needs of a given application. SNAs can be composed of a variety of oligonucleotides (e.g., DNA, siRNA, microRNA, peptide nucleic acid (PNA), or locked nucleic acid (LNA)) and a variety of different types of nanoparticle cores, such as gold (Au) [34], silver (Ag) [46], iron oxide (Fe_3O_4) [47, 48], quantum dots (CdSe, CdSe/ZnS) [49, 48], platinum [48], silica (SiO_2) [50], core-shell ($Au@SiO_2$) [50], and liposomes [51] typically ranging in size from 10 to 50 nm. Coreless versions of these structures can also be made that display the same useful properties as the core-filled structures, emphasizing the concept that the properties of SNAs stem from their densely functionalized and highly oriented nucleic acid shell and not from the nanoparticle core [51–54]. Some types of the hollow SNAs that have been synthesized thus far include those consisting of cross-linked oligonucleotides [53], DNA-block copolymer micelles [55, 56], infinite coordination polymers [52], metal organic frameworks [54], and liposomes [51]. Hollow SNAs, such as the liposomal SNAs, represent an exciting new class of metal-free SNAs that can be useful in gene regulation, and their potential is only beginning to be realized [51]. The liposomal SNAs have some exciting advantages over conventional liposomal structures, as the oligonucleotide cargo is arranged on the surface of the liposomal entity and thus stabilizes liposomes in the sub-100 nm range. Other synthetic advances in SNA development include the ability to attach RNA to DNA-based SNAs via enzymatic ligation to create RNA-DNA hybrid SNAs [57]. These structures can be used to regulate gene

expression in a manner similar to other types of SNAs, and they are more cost-effective to synthesize than SNAs composed solely of RNA oligonucleotides. SNAs can also be backfilled with a variety of surface passivating molecules, such as polyethylene glycol (PEG) [40, 45] or oligoethylene glycol (OEG) [41, 45], which have been known to improve colloidal stability, increase circulation time, and reduce protein adsorption [58, 59].

1.5 Applications of SNAs in Cancer Research and Treatment

The ability to tune the oligonucleotide sequence of SNAs is extremely powerful in the development of SNAs as cancer therapeutics. For example, treatment with SNAs in vitro has resulted in gene knockdown of model targets, such as luciferase [41] and enhanced green fluorescent protein (eGFP) [42, 50], as well as targets involved in cancer cell growth and proliferation, such as HER2 (an oncogenic receptor tyrosine kinase (RTK) responsible for development and progression of cancers, in particular breast cancers) [51, 60], *Bcl2L12* (a GBM oncoprotein and potent inhibitor of effector caspases and p53) [45], and epidermal growth factor receptor (EGFR; a RTK that is important for maintaining epidermal homeostasis and a potent oncogene in several cancers when overexpressed or mutated [61] both in vitro and in vivo). Because the oligonucleotide sequence can be designed to target virtually any mRNA of interest, we have only begun to scratch the surface of the potential of SNAs as cancer therapeutics; SNAs could theoretically be used to target any disease with a genetic basis, including many forms of cancer. To illustrate this versatility, we will highlight three applications below in which SNAs are used to treat cancer. First, we will highlight how SNAs can be used in the treatment of glioblastoma multiforme (GBM), the most prevalent and aggressive form of primary central nervous system malignancies. Then, we will discuss how SNAs can be delivered topically to regulate EGFR in the treatment of hyperproliferative skin disorders and skin cancer. Finally, we explore SNAs as multifunctional therapeutic agents, where drug conjugation to the SNA results in the simultaneous delivery of oligonucleotides and drugs. These structures are being evaluated for the treatment of prostate and breast cancer.

2 SNAs for the Treatment of Glioblastoma Multiforme (GBM)

2.1 *Bcl2L12*-Targeting siRNA SNAs

Due to the unabated growth of GBM tumors and their extensive resistance to therapies, only 3–5 % of patients survive longer than 3 years postdiagnosis [62]. Most therapeutics tested to treat GBM do not penetrate the blood–brain barrier/blood–tumor barrier (BBB/BTB) and therefore are extremely ineffective [63]. However, given that SNAs are rapidly taken up by scavenger receptors, including

those found on the surface of endothelial cells of the BBB/BTB, SNAs merited investigation as a therapeutic platform that could cross the BBB/BTB and pervasively penetrate glioma tissue [64, 65]. To preclinically evaluate SNAs for the treatment of GBM, Jensen et al. utilized an in vitro co-culture model of the human BBB, consisting of human primary brain microvascular endothelial cells (huBMECs) and human astrocytes [45]. The authors designed SNAs consisting of a 13 nm gold nanoparticle core conjugated to thiolated siRNA duplexes targeting the GBM oncogene *Bcl2L12*, an effector caspase and p53 inhibitor overexpressed in the vast majority (>90 %) of GBM tumors [66–70]. By labeling these SNAs with a fluorescent Cy5.5 dye and employing fluorescence microscopy, the authors

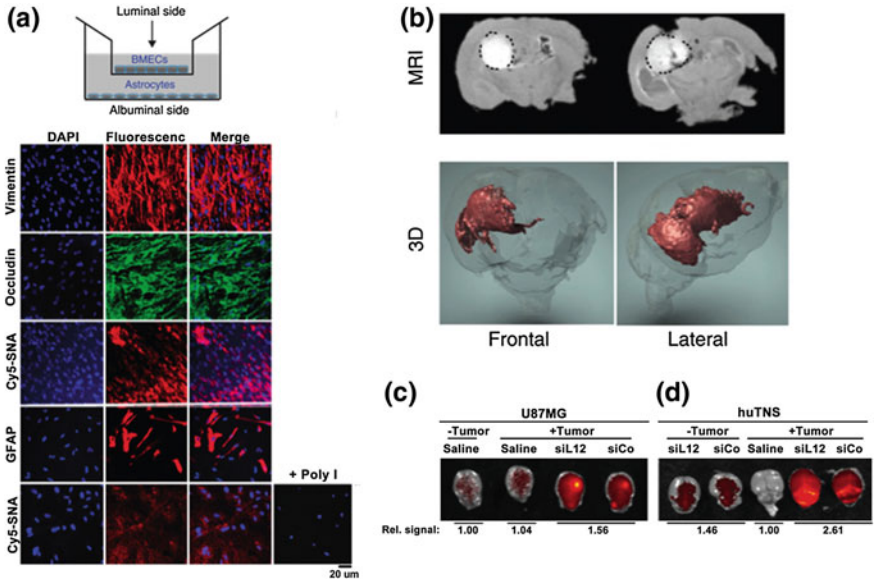

Fig. 4 *BcL2L12*-SNAs in treatment of glioblastoma multiforme. SNAs cross the BBB/BTB and selectively accumulate in glioma tissue. **a** Noncontact in vitro BBB model using a co-culture of human primary brain microvascular endothelial cells (huBMECs) and human astrocytes. Representative confocal fluorescence microscopy images demonstrate Cy5.5-SNA (*red*) distribution in endothelial and astrocytic cells. Endothelial and astrocytic cells stained positively for occludin (a marker for tight junctions) and glial fibrillary acidic protein (GFAP), respectively. The cytoplasm is stained with DAPI and the nuclei stained with anti-vimentin; **b** Magnetic resonance (MR) images of tumor-bearing mouse brains injected intracranially with SNAs-Gd^{III}. Two representative coronal sections imaged 24 h after SNAs-Gd^{III} injection (*upper panel*) show localization of SNAs-Gd^{III} within the intracerebral lesion. Gd^{III} *signal is white* and *outlined* with a *black dotted line*. Also shown is the corresponding three-dimensional (3D) reconstruction of MR images (Gd^{III} *signal in red*); **c** and **d** IVIS analysis of brains with or without human glioblastoma-astrocytoma (U87MG) (**c**) or human tumor neurospheres (huTNS) (**d**) tumors 48 h after systemic delivery of saline or Cy5.5-SNAs. SNA accumulation is indicated by increased fluorescence (*yellow*). Quantification of radiant efficiency is shown as relative signal amount under the images. SiCo = scrambled control sequences. Adapted with permission from Jensen et al. [45]. Copyright 2013. *Science Translational Medicine*

demonstrated that *Bcl2L12*-targeting SNAs (*L12*-SNAs) were able to undergo transcytosis through the huBMEC layer and enter human astrocytes (Fig. 4a) [71–73]. Consistent with the previous reports of SR-A-mediated uptake of SNAs [36, 37], this BBB-penetrating capacity was abolished when polyinosinic acid (Poly-I), which blocks SR-A-dependent SNA uptake and likely mediates transcytosis, was added prior to SNA treatment. Next, BBB and glioma tissue penetration was evaluated in vivo in both healthy and glioma-bearing mice. In conjunction with Cy-5 dye, gadolinium (Gd^{III}) was conjugated to SNAs to visualize and quantify their tissue penetration; the biodistribution of these SNAs was evaluated via inductively coupled plasma-mass spectrometry (ICP-MS), magnetic resonance imaging (MRI), and confocal fluorescence microscopy. Gd^{III}-SNA conjugates were prepared from alkyne-modified DNA thymine (dT) nucleotides and azide-labeled Gd^{III} complexes through click chemistry. Following local administration, both 3D reconstruction of MRI images and confocal fluorescence demonstrated extensive intratumoral dissemination by SNAs (Fig. 4b). ICP-MS further validated these results, showing a 10-fold higher accumulation of SNAs in tumor versus nontumor brain regions, possibly due to the enhanced permeation and retention (EPR) effect [74]. Following tail vein injection of Cy5.5-labeled *L12*-SNAs, in vivo imaging system (IVIS) quantification of radiant intensities showed a 1.8-fold higher accumulation of SNAs in GBM-xenograft-bearing mice compared to sham GBM-inoculated mice (Fig. 4c). Furthermore, systemically delivered *L12*-SNAs successfully neutralized *Bcl2L12* expression, increased intratumoral apoptosis, reduced tumor burden, and increased survival. Systemically administered *L12*-SNAs did not induce inflammatory cytokines, cause any changes in blood chemistry and complete blood counts, or elicit changes in histopathology compared to saline or control SNAs. With no evidence to date of toxicity and promising in vivo results thus far, *L12*-SNAs represent a promising construct for GBM treatment that is headed toward early clinical testing.

2.2 Delivery of Therapeutic miRNA Using miR-182 SNAs

miRNAs have been shown to be important regulators of GBM pathogenesis and therapeutic susceptibility [75]. Genomic studies have characterized miRNA-controlled signaling pathways, which include critical growth and survival pathways, such as receptor tyrosine kinase (RTK)-phosphoinositide 3-kinase (PI3K)-phosphatase and tensin homolog (PTEN), retinoblastoma (Rb), B-cell lymphoma 2 (Bcl-2), and tumor protein p53 (p53) signaling pathways [76, 77]. Given the global overexpression of *Bcl2L12*, its roles in the pathogenesis of GBM, and its involvement in therapy resistance, the Kessler, Peters, Mirkin, and Stegh labs sought to identify miRNAs that control the expression of *Bcl2L12* in GBM [78]. In silico studies of GBM samples from the multidimensional Cancer Genome Atlas (TCGA) dataset (http://cancergenome.nih.gov/dataportal/) were designed to discover miRNAs with expression levels negatively correlated with *Bcl2L12* mRNA levels (Cancer Genome Atlas Research [79]. From these studies, miR-182 was identified as a potential miRNA candidate that regulates *Bcl2L12* expression.

The authors demonstrated that miR-182 acts as a tumor suppressor in GBM by not only controlling the expression and activity of *Bcl2L12*, but also levels of the RTK c-Met and the transcription factor hypoxia-inducible factor 2α (HIF2α). To harness miR-182-related tumor suppressive functions as a therapeutic in vitro and in vivo, the authors synthesized SNAs functionalized with mature miR-182 sequences (182-SNAs). Treatment of glioma cells with 182-SNAs in vitro was shown to potently decrease *Bcl2L12* and c-Met protein levels compared to control SNA-treated cultures, while substantially increasing apoptotic responses and reducing cellular growth. The authors then evaluated 182-SNAs in mice bearing orthotopic GBM xenografts in vivo. In 182-SNA-treated mice compared to control SNA-treated mice, average tumor weights were reduced, and 182-SNA-treated mice experienced significantly prolonged survival relative to control SNA-treated mice.

Taken together, 182-SNAs were shown to effectively decrease *Bcl2L12* and c-Met protein levels, enhance apoptotic responses to chemotherapy, drastically reduce tumor burden, and extend survival of GBM-xenograft-bearing mice. Coupled with the absence of any observable side effects or toxicity, 182-SNAs represent a novel platform for delivering therapeutic miRNAs in GBM.

3 Topical Delivery of SNAs to Regulate Epidermal Growth Factor Receptor (EGFR)

In order to suppress cancer-causing genes in the skin using oligonucleotides, the oligonucleotide must pass the epidermal barrier. One of the greatest challenges associated with topical drug delivery is the design and synthesis of materials that can pass through this barrier [80–82]. In skin, topical delivery is the desired route for delivering agents that can regulate gene suppression because the skin is easily accessible and because topical delivery reduces the risk of systemic side effects. Therefore, an agent that can deliver oligonucleotides through the epidermal barrier with relatively little cytotoxicity would be ideal. Recently, it has been shown that SNAs can be delivered topically in a commercial moisturizer or phosphate buffered saline (PBS) solution to target EGFR, an important gene for epidermal homeostasis and potent oncogene that is frequently overexpressed or mutated in cancer [83, 84]. SNAs were able to penetrate through hairless mice and human skin equivalents without any clinical or histological evidence of toxicity [39]. The Mirkin and Paller labs first measured the uptake of SNAs in normal human keratinocytes (hKCs) because they are notoriously difficult to transfect [85]. ICP-MS revealed that SNA uptake is five times higher in hKCs as compared to HaCaT (spontaneously immortalized hKCs) or HeLa cells [39]. Although the underlying mechanism for the high cellular uptake in hKCs is still under investigation, these data show the potential of SNAs as a strong candidate for topical oligonucleotide delivery. When the uptake in hKCs was visualized by confocal microscopy using nontargeting SNAs with a Cy3 dye, strong fluorescence was seen in the cytoplasm of the cells

and morphological differences were not seen between untreated hKCs and SNA-treated hKCs (Fig. 5a). To determine potential off-target effects of SNAs, genome-wide expression profiling revealed only seven up-regulated genes (none were downregulated); in contrast, 427 genes were up- or down-regulated in the case of lipid-based siRNA delivery using the DharmaFECT1™® transfection reagent. This is a promising result because SNA toxicity should be relatively low since there are virtually no off-target effects.

After confirming that SNAs enter hKCs and cause relatively little immune response, the potential for EGFR mRNA and protein knockdown was assessed. Western blot analysis showed that there was greater EGFR suppression by 0.3 nM siRNA delivered by SNA than 30 nM siRNA delivered by DharmaFECT1™ in hKCs (Fig. 5b). In fact, total suppression of EGFR, as seen by Western blot, was observed with incubation of 1.5 nM total siRNA delivered by SNAs, something that was not seen even at 30 nM siRNA delivered by DharmaFECT1™, thus demonstrating the potency of oligonucleotide delivery via SNAs.

The authors then investigated the potential of SNAs to penetrate mouse skin. In both SKH10E hairless mice and hair-bearing C57BL/6 J mice that were shaved 24 h before treatment, SNA penetration through the stratum corneum and into the epidermis and dermis was seen in as few as 3 h after a single SNA dose (Fig. 5c). Furthermore, after treating SKH1-E hairless mice daily for 3 days with nontargeting SNAs and monitoring the gold content in skin for 10 days post-treatment, it was found that only 2 % of the initial gold was still present in the skin (Fig. 5d). In summary, SNAs were shown to penetrate the skin of two different mice strains and subsequently clear the skin by 10 days post-treatment.

The next step was to investigate the efficacy of EGFP suppression in mouse skin. Western blot analysis showed that the protein expression of EGFP was nearly eliminated and the downstream phosphorylation of ERK was inhibited by 74 % from the application of SNAs in Aquaphor®; Aquaphor® alone, nontargeting SNAs, and free siRNA did not have an effect on EGFP expression (Fig. 5e). Furthermore, the decrease in EGFP expression was accompanied by a 74 % decrease in the phosphorylation of downstream extracellular signal-regulated kinases (ERK1/2), demonstrating the specificity of EGFR knockdown (total ERK1/2 expression remained constant). To confirm the phenotypic effect of EGFR knockdown on mouse skin, computerized morphometric analysis of histological sections of mouse skin treated with EGFR SNAs showed an almost 40 % reduction in thickness compared to the mouse skin treated with Aquaphor® alone or nontargeting SNAs (Fig. 5c). Similar results were seen with human skin equivalents. Taken together, these data demonstrate the ability of SNAs to knockdown a specific gene target in vivo, which causes a specific biological response with minimal off-target effects. This study lays the groundwork for SNAs to be utilized for topical oligonucleotide delivery with vast potential in the treatment of skin diseases and disorders, such as metastatic melanoma and psoriasis.

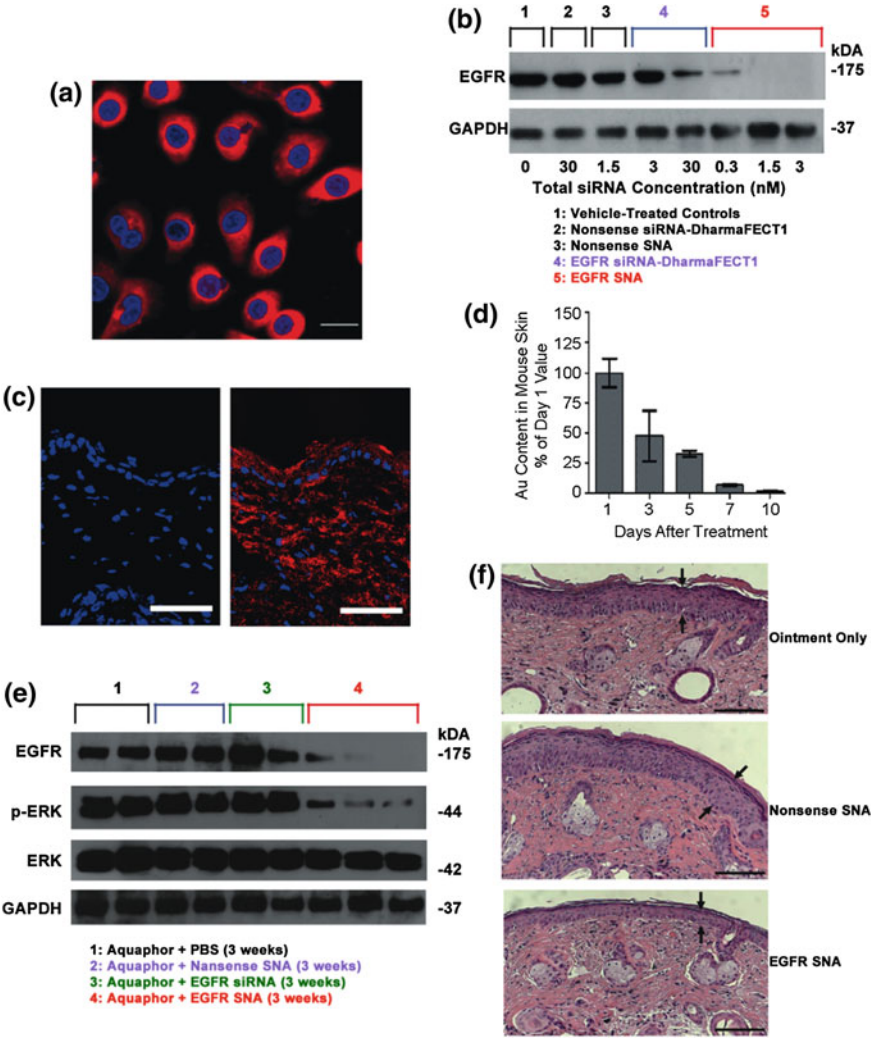
(a)
(b)
1 2 3 4 5
kDA
EGFR
-175
GAPDH
-37
0 30 1.5 3 30 0.3 1.5 3
Total siRNA Concentration (nM)
1: Vehicle-Treated Controls
2: Nonsense siRNA-DharmaFECT1
3: Nonsense SNA
4: EGFR siRNA-DharmaFECT1
5: EGFR SNA
(c)
(d)
Au Content in Mouse Skin
% of Day 1 Value
150
125
100
75
50
25
0
1 3 5 7 10
Days After Treatment
(e)
1 2 3 4
EGFR
p-ERK
ERK
GAPDH
kDA
-175
-44
-42
-37
1: Aquaphor + PBS (3 weeks)
2: Aquaphor + Nansense SNA (3 weeks)
3: Aquaphor + EGFR siRNA (3 weeks)
4: Aquaphor + EGFR SNA (3 weeks)
(f)
Ointment Only
Nonsense SNA
EGFR SNA

◀ **Fig. 5** Topical delivery of SNAs through human and mouse skin. **a** Uptake of Cy3-labeled nonsense SNAs (*red*) in the cytoplasm of approximately 100 % of the primary human keratinocytes (hKCs) after 24 h incubation. The nuclei were stained *blue* with Hoechst 33343. Scale bar, 20 μm; **b** Western blot showing epidermal growth factor receptor (EGFR) protein levels for hKCs treated for 48 h. Note the greater suppression by 0.01 nM EGFR SNAs (equivalent to 0.3 nM siRNA) as compared with the 30 nM EGFR siRNA delivered with DharmaFECT1™ at 60 h; **c** Mouse (SKH1-E) skin treated topically with 1:1 Aquaphor® only (*left*) or with 50 nM Cy5-labeled (*red*) SNAs dispersed in the 1:1 Aquaphor® (*right*). The SNAs are seen in the cytoplasm of epidermal cells and the dermis 3 h after application. DAPI-stained nuclei in blue. Scale bars, 100 μm; **d** Mouse skin was treated daily for 3 days with nonsense SNAs and analyzed by ICP-MS for gold content. The gold content in mouse skin progressively decreases after cessation of topical treatment; 10 days after the final treatment, only 2 % of the original gold content remains ($n = 3$ at each time point); **e** The protein expression of EGFR was nearly eliminated in the EGFR SNA-treated group, whereas the downstream phosphorylation of ERK was inhibited by 74 %; total ERK expression remained constant; **f** The mean thickness of EGFR SNA-treated skin was 40 % less than that of control-treated skin ($P < 0.001$), as measured by computerized morphometry. Epidermal thickness was measured from the top of the stratum granulosum to the basement membrane (*arrows*) at three equidistant sites. Adapted with permission from Zheng et al. [39]. Copyright 2012. *Proceedings of the National Academy of Sciences of the United States*

4 Multifunctional SNAs

Thus far, we have discussed SNAs that enter cells and tumor tissues and perform a single function (e.g., regulate gene expression via the RNAi or antisense pathway). However, SNAs that can perform multiple therapeutic, diagnostic, targeting, and imaging functionalities simultaneously within a cell can also be synthesized. Using solid-phase DNA synthesis, modified phosphoramidites can be used to add specific chemical functional groups onto oligonucleotides; and these functional groups can be used as handles to attach drugs, small molecules, or antibodies of interest to these oligonucleotides. When these modified oligonucleotides are formulated as SNAs, the SNA structure allows for the cellular entry of the conjugate and the oligonucleotides allow for the regulation of gene expression, while the small molecule drug or contrast agent that is appended to the oligonucleotides that comprise the SNAs, for example, can be used as an additional therapeutic component or imaging modality, respectively.

4.1 SNA-Drug Conjugates for Drug Delivery

Cisplatin and carboplatin are widely regarded as effective treatments for testicular and ovarian cancers, and these drugs have also been utilized for the treatment of bladder, cervical, head and neck, esophageal, and small cell lung cancer [86, 87]. However, many of the synthetic delivery systems used for cisplatin and carboplatin are associated with systemic toxicity [88]. Because SNAs have been shown to enter cells in high quantities [35] without provoking a significant immune response [38],

they are a promising platform for the delivery of these and other platinum (Pt) compounds. To this end, the Lippard and Mirkin labs collaborated to synthesize a DNA oligonucleotide with a terminal dodecyl amine to which the Pt (IV) pro drug (*c,c,t*-{$Pt(NH_3)_2Cl_2(OH)(O_2CCH_2CH_2CO_2H$}) was conjugated via amide linkages (Fig. 6a) [89]. Platinum atomic absorption spectroscopy (AAS) showed that 98 % of the DNA amines on the SNA were conjugated to platinum. The mechanism of action for Pt (IV) complexes requires that they are reduced to cytotoxic Pt (II) in a reducing environment, such as inside cells or blood [90]. Electrochemical studies confirmed that the conjugation of a Pt (IV) payload to the SNA did not significantly alter the reduction potential of the complex, making it likely that the axial ligands of the Pt (IV) complex could be removed once it entered a reducing environment. It was also confirmed that the SNAs still entered HeLa cervical cancer cells with the Pt (IV) prodrugs attached (Fig. 6b), and specifically colocalized with microtubules

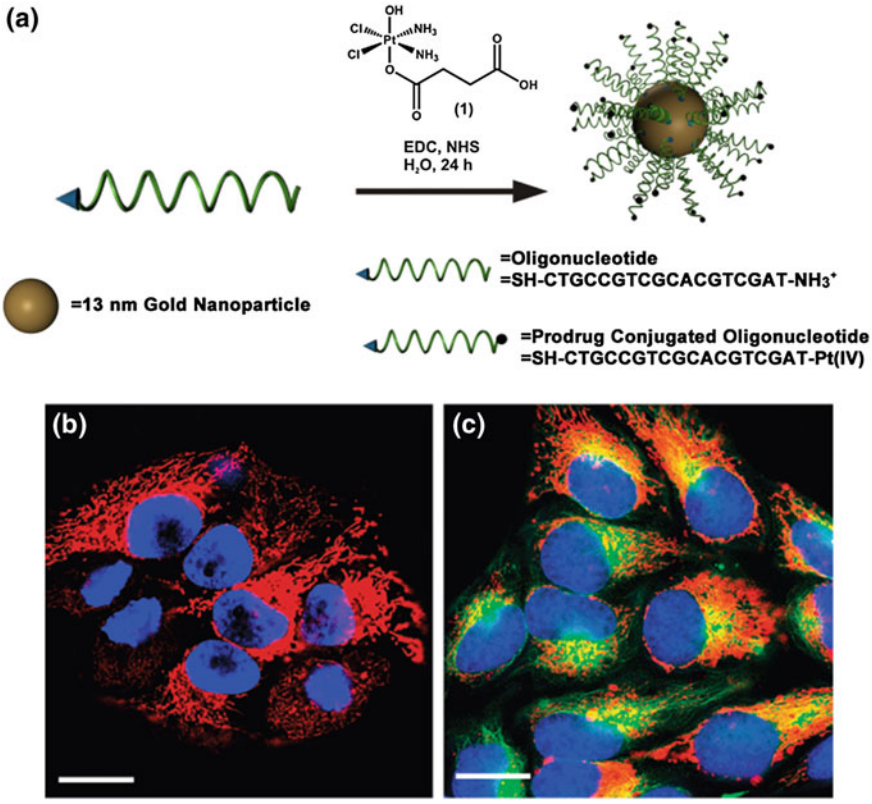

Fig. 6 Drug and oligonucleotide dual therapy. **a** Scheme for the synthesis of Pt (IV) terminated SNAs; **b** Live cell imaging of HeLa cells upon incubation with platinum-tethered Cy5-SNAs for 12 h; **c** Co-localization of the particles with the cytoplasmic microtubules. Hoechst 33342 was used for nuclear staining. Scale bars, 20 μm. Adapted with permission from Dhar et al. [89]. Copyright 2009. American Chemical Society

(Fig. 6c). Finally, the efficacy of the SNA-bound Pt (IV) prodrug was assessed in four different cell lines. For A549 lung epithelial cancer cells in particular, the conjugation of the Pt (IV) prodrug to the SNA resulted in superior killing efficiency, with a half maximal inhibitory concentration (IC_{50}) of 0.9 μM, compared to an IC_{50} of 11 μM for free cisplatin. Therefore, it appears that the Pt (IV) prodrug is more effective when conjugated to DNA on the SNA surface. Future work will include using the oligonucleotide, whether it is DNA or RNA, to knockdown gene expression, which, in conjunction with drug delivery, should render these constructs even more effective.

The Ho and Mirkin labs employed a similar strategy with the chemotherapeutic Paclitaxel [91]. Paclitaxel is used to treat cancers such as ovarian, breast, and nonsmall cell lung cancers [92, 93]. Paclitaxel is challenging to deliver because of its low aqueous solubility; cells also acquire chemoresistance toward this drug and it often causes harmful side effects [94]. Therefore, it was hypothesized that Paclitaxel's conjugation to SNAs may increase its aqueous solubility and perhaps decrease the associated side effects.

Zhang and co-workers conjugated a thiolated oligonucleotide containing a terminal Paclitaxel group to 13 nm gold nanoparticles (AuNPs) (Fig. 7a; compound 3) [91]. This step was accomplished by modifying Paclitaxel molecules with succinic anhydride groups to form a Paclitaxel carboxylic acid derivative (compound 1), which was conjugated to DNA oligonucleotides with a terminal amine group using EDC/sulfo-NHS chemistry (compound 2). The average number of Paclitaxel molecules per gold nanoparticle was measured to be 59 ± 8. It is interesting to note that while free Paclitaxel is not soluble in phosphate buffered saline (PBS) at a 5 μM concentration, the SNA-Paclitaxel conjugates remain well dispersed in PBS, as confirmed by dynamic light scattering (DLS) (Fig. 7b) and transmission electron microscopy (Fig. 7c). Free Paclitaxel has a maximum solubility of 0.4 μg/mL in aqueous solution [95] and the SNA-Paclitaxel conjugate exhibits a maximum solubility for Paclitaxel of 21.35 μg/mL, a greater than 50-fold enhancement in drug solubility. Confocal microscopy confirmed the internalization of fluorophore-labeled SNA-Paclitaxel conjugates in MCF7 human breast adenocarcinoma cells and MES-SA/Dx5 human uterine sarcoma cells after a 6 h incubation. A terminal deoxynucleotidyl transferase dUTP nick end-labeling (TUNEL) assay [96] determined that DNA fragmentation and apoptosis was induced by Paclitaxel. It was shown that Paclitaxel remained active when bound to SNAs and that the SNA-Paclitaxel conjugates have the potential to overcome Paclitaxel resistance in cells.

Furthermore, the ability of SNA-Paclitaxel conjugates to kill cancer cells derived from different types of cancer (MCF7 breast cancer cells, MES-SA/Dx5 multidrug resistant cells derived from uterine sarcoma, and SKOV-3 ovarian cancer cells) was assessed. Enhanced cytotoxicity was observed in all three cell lines for the SNA-Paclitaxel conjugate when compared with free Paclitaxel and the DNA-Paclitaxel conjugate. Therefore, the SNA formulation of Paclitaxel may overcome the cellular cross-resistance of chemotherapeutics in vitro. There are also significant advantages to using the SNA-Paclitaxel formulation compared to the free Paclitaxel and the DNA-Paclitaxel conjugate when looking at the IC_{50} (in nM Paclitaxel; Table 1). In

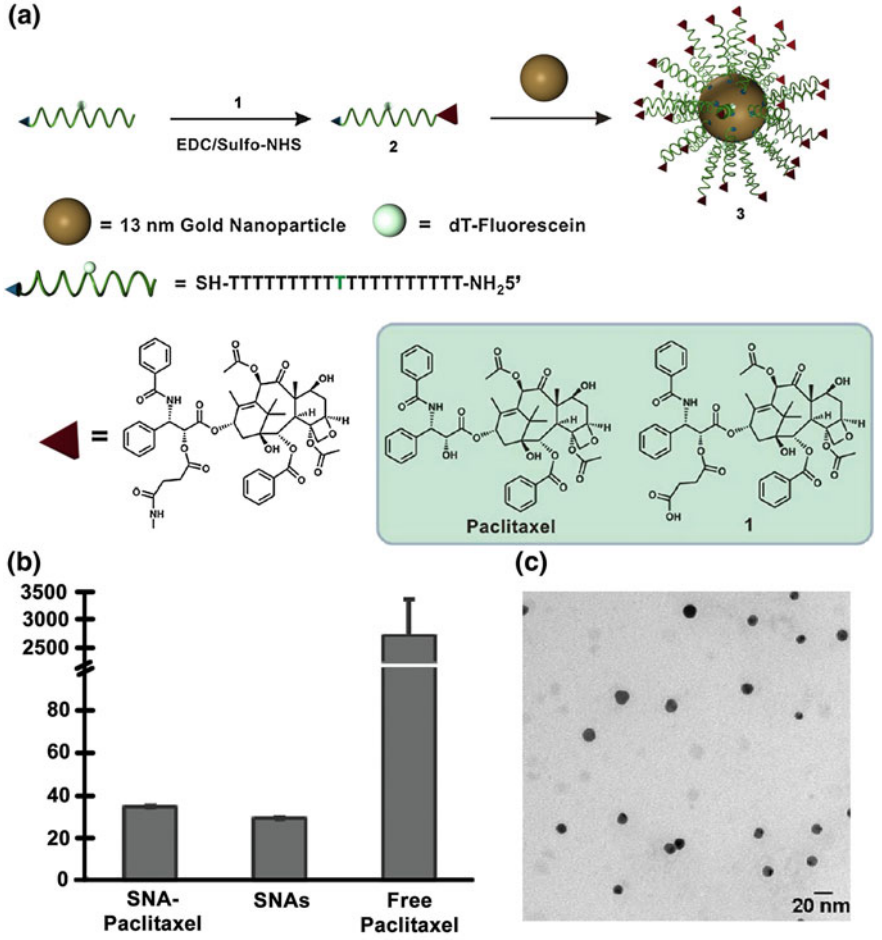

Fig. 7 Drug solubility and efficacy of paclitaxel increases upon covalent linkage with SNAs. **a** Synthesis of SNA-Paclitaxel conjugates; **b** Hydrodynamic sizes of SNA-Paclitaxel conjugates (3), SNAs, and Paclitaxel in PBS buffer ($n = 3$). The compounds were suspended in PBS buffer at the equivalent Paclitaxel concentration of 21.3 μg/mL (25 μM) for dynamic light scattering (DLS) measurement; **c** TEM image of SNA-Paclitaxel conjugates (3). Scale bar is 20 nm. Adapted with permission from Zhang et al. [91]. Copyright 2011. *ACS Nano*

MCF7 cells, for example, the IC_{50} decreases from above 1 μM and 193 nM for free Paclitaxel to 119.4 and 52.6 nM for SNA-Paclitaxel conjugates after 12 and 48 h, respectively. Therefore, conjugation to SNAs represents a potential new route to solubilize previously insoluble drugs and improve their biological response. Future work is still needed to better understand the mechanism of enhanced efficacy in this system, but the groundwork has been set for the use of SNAs as platforms to which other biologically relevant small molecules can be conjugated.

Table 1 IC_{50} of SNA-Paclitaxel conjugates (3), free Paclitaxel, and compound (1) after 12 and 48 h Incubation in MCF7 Breast cancer, SKOV-3 Ovarian Cancer, and MES-SA/Dx5 multidrug resistant cells

Cell line	Incubation time (h)	IC_{50} (nM Paclitaxel)		
		SNA-Paclitaxel	Paclitaxel	Paclitaxel carboxylic acid derivative
MCF7	12	119.4	>1000	>1000
	48	52.6	193.0	133.2
SKOV-3	12	4.3	175.6	>1000
	48	17.5	28.9	188.0
MES-SA/Dx5	12	118.0	>1000	>1000
	48	104.5	>1000	>1000

Adapted with permission from Zhang et al. [91]. Copyright 2011. *ACS Nano*

4.2 SNA-Antibody Conjugates for Cellular Targeting

While SNAs solve many challenges associated with the intracellular delivery of oligonucleotides, the fact that they allow entry into most cells in a nonspecific fashion could present a problem in the targeting of genes essential for normal organ homeostasis. To enhance SNA association with target cells, the Mirkin lab conjugated a monoclonal antibody (mAb) designed to bind to the human epithelial growth factor receptor 2 (HER2) to antisense DNA-SNAs to create HER2-targeting antisense DNA-SNAs [60]. HER2 is involved in signal transduction pathways leading to increased cellular growth and differentiation, and it is up-regulated in many epithelial cancers, including breast, ovarian, gastric, and salivary [97, 98]. The authors utilized copper (I) (Cu(I)) click chemistry to conjugate a HER2 antibody to antisense DNA, specifically linking an azide-functionalized HER2 mAb to DNA with a 3′ alkyne group (Fig. 8a).

Using ICP-MS, the authors evaluated the cell uptake of both HER2-targeted and nontargeted SNAs as a function of time in HER2 overexpressing SKOV-3 ovarian cancer cells (Fig. 8b). In the first 6 h of incubation, the HER2-targeted SNAs demonstrated a significantly higher rate of uptake compared to the nontargeted SNAs ($\sim$236 particles s^{-1} $cell^{-1}$ for HER2-targeted SNAs vs. $\sim$19 particles s^{-1} $cell^{-1}$ for nontargeted SNAs). However, as incubation time was extended to 24 h, the selectivity diminished, perhaps due to the cells' inability to replenish HER2 on their surfaces after mAb binding and endocytosis [99]. Furthermore, band density analysis by Western blot for HER2-targeted SNAs in SKOV-3 cells revealed that at certain concentrations, HER2 expression could no longer be detected (Fig. 8c). Thus, HER2-targeting SNAs were taken up by HER2 over expressing cells to a greater extent and at a faster initial rate compared to nontargeted particles. Additionally, HER2-targeting SNAs demonstrated potent antisense gene knockdown, requiring only pM amounts of SNAs to drastically silence HER2

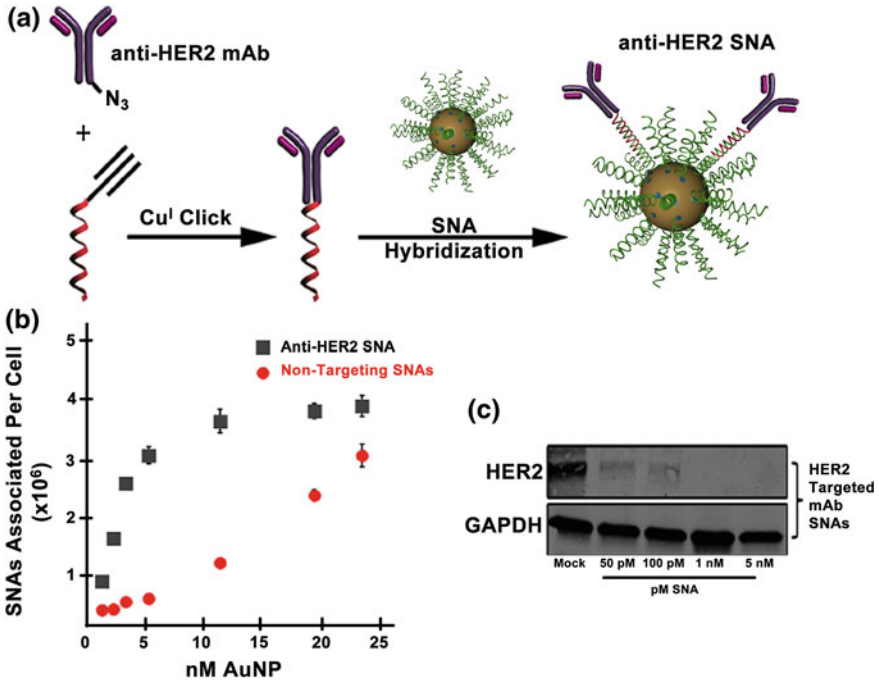

Fig. 8 Human epidermal growth factor receptor 2 (HER2)-targeted SNAs. **a** Synthesis of HER2-targeting SNAs; **b** Cell uptake of targeted versus nontargeted SNAs in SKOV-3 ovarian cancer cells as a function of time; **c** Western blot of HER2 expression in SKOV-3 cells after treatment with increasing concentrations of HER2-targeting SNAs. GAPDH is used as an internal reference. Adapted with permission from Zhang et al. [60]. Copyright 2012. American Chemical Society

expression. Hence, these SNA-antibody constructs are capable of increasing both the selectivity and efficacy of the SNA platform.

4.3 Gadolinium-Enriched SNAs for Cellular Imaging

The Meade and Mirkin labs utilized SNAs as a platform to synthesize bioactivated contrast agents that are capable of penetrating cells for use in cell-tracking experiments [100]. The most commonly used contrast agents, paramagnetic gadolinium (III) (Gd^{III}) complexes, are advantageous because Gd^{III} complexes have high relaxivities since they reduce the longitudinal relaxation time (T_1) of local water protons [101]. Song and co-workers sought to fill the need for a magnetic resonance imaging (MRI) agent with both high Gd^{III} loading (for enhanced contrast) and efficient cellular uptake (for imaging small cell populations) by conjugating Gd^{III} to SNAs [100]. The Gd^{III} complexes were attached through click chemistry to poly DNA thymine (poly dT) oligonucleotides, which contained five conjugation sites of hexylamino labeled DNA thymine (dT groups conjugated with a cross-linker,

azidobutyrate-*N*-hydroxysuccinimidester) (Fig. 9a). Through ICP-MS, the Gd^{III} loading per SNA was calculated; there were 342 ± 1 Gd^{III} per 13 nm AuNP and 656 ± 20 Gd^{III} per 30 nm AuNP. The relaxation efficiencies of DOTA-Gd^{III}, DNA-Gd^{III}, and SNA-Gd^{III} (13 and 30 nm AuNPs) were measured by taking the slope of a plot of the measured $1/T_1$ as a function of Gd^{III} concentration (Table 2). The relaxivity at 37 °C in water at 60 MHz increased from 3.2 mM^{-1} s^{-1} for DOTA-Gd^{III} to 8.7 mM^{-1} s^{-1} for DNA-Gd^{III} to 16.9 mM^{-1} s^{-1} for 13 nm SNA-Gd^{III} and 20.0 mM^{-1} s^{-1} for 30 nm SNA-Gd^{III}. These results are consistent with the Soloman-Bloembergen-Morgan theory, which states that there is a concomitant decrease in rotational correlation time (τ_r) with an increase in r_1 [102–106]. T_1 weighted MR images in solution phantoms as well as NIH/3T3 mouse fibroblast cells show that SNA-Gd^{III} is significantly brighter than DOTA-Gd^{III} at multiple

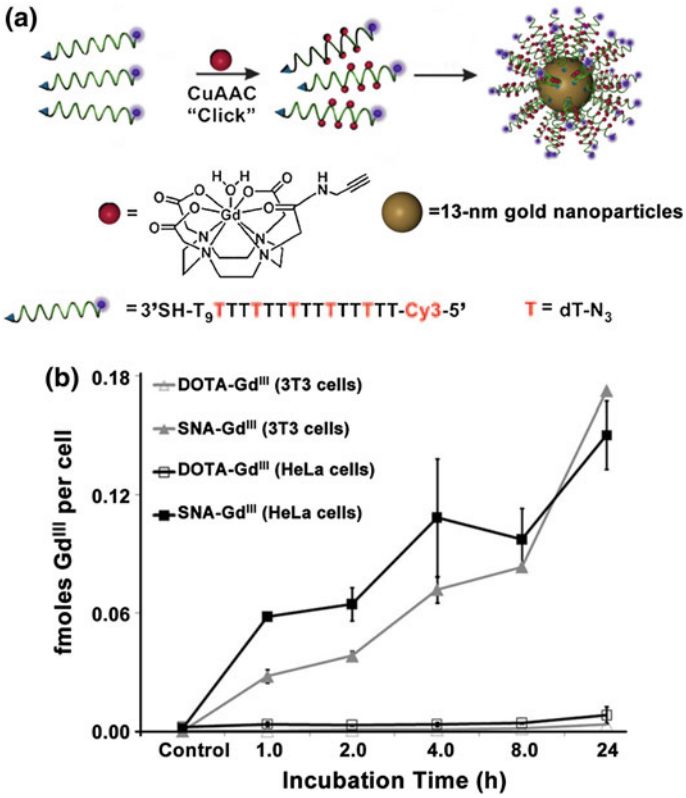

Fig. 9 Multimodal SNA-Gd^{III}. **a** Synthesis of Cy3-SNA-Gd^{III} conjugates using copper catalyzed azide alkyne cycloaddition (CuAAC); **b** Time-dependent cellular uptake of SNA-Gd^{III} conjugates compared to DOTA–Gd^{III} in NIH/3T3 mouse fibroblast and HeLa cervical cancer cells. Cells were incubated with 6.5 μM Gd^{III} for both contrast agents. Error bars represent ±1 standard deviation of the mean for duplicate experiments. Adapted with permission from Song et al. [100]. Copyright 2009. *Angewandte Chemie*

Table 2 Relaxivities (r) of Gd^{III} complexes and conjugates at 60 and 600 MHz

	r_1, (mM^{-1} s^{-1})	
	60 MHz (1.41 T)	600 MHz (14.1 T)
DOTA-Gd^{III}	3.2[a]	2.2
DNA-Gd^{III}	8.7	NM
13 nm SNA-Gd^{III}/ionic	16.9	5.1
13 nm SNA-Gd^{III}/particle	5779	1275
30 nm SNA-Gd^{III}/ionic	20.0	NM
30 nm SNA-Gd^{III}/particle	13,120	NM

60 MHz measured in pure water at 37 °C and 600 MHz measured in cell media at 25 °C. NM = not measured

[a]Taken from [107]

Adapted with permission from Song et al. [100]. Copyright 2009. *Angewandte Chemie*

Gd^{III} concentrations. To confirm efficiency of cellular uptake, NIH/3T3 and HeLa cells were incubated with SNA-Gd^{III} or DOTA-Gd^{III} for increasing amounts of time. At all concentrations, the Gd^{III} uptake was more than 50-fold higher for SNA-Gd^{III} than for DOTA-Gd^{III} (Fig. 9b). Therefore, SNAs functionalized with Gd^{III} are outstanding contrast agents that freely enter cells.

Finally, the cell labeling efficiency was assessed using analytical flow cytometry. It was found that incubation of Cy3 SNA-Gd^{III} with NIH/3T3 cells results in 80 and 100 % of the cells being labeled after four and 24 h, respectively. Taken together, these data demonstrate the versatility of the SNA platform and show that conjugation of Gd^{III} to SNAs results in a multimodal, cell permeable MR contrast agent that is biocompatible, has a high Gd^{III} loading, and relatively high relaxivity. These Gd-SNA conjugates also show a greater than 50-fold increase in cell uptake compared to clinically available DOTA-Gd^{III}. When also designed and synthesized to target a gene of interest, such SNAs could be efficiently used as dual imaging-therapeutic moieties.

4.4 Self-Assembled, Multimodal SNAs for Cancer Therapy

The design of multimodal nanomaterials (i.e., nanoconjugates capable of simultaneously performing various functions including imaging, sensing, and drug delivery) is becoming increasingly desired. As such, the Tan lab sought to further expand the multimodal potential of SNAs by generating self-assembled, SNA-based constructs that combine fluorescent imaging, specific target cell recognition, and high drug loading capacity [108]. To achieve this, 30 nm streptavidin magnetic nanoparticles (MNPs) were conjugated with a biotin-DNA initiator strand that triggered a cascade of DNA-assisted hybridization reactions of monomer DNA sequences, resulting in the formation of a long DNA polymer (diameter after assembly $\sim$124 nm) as the nanoparticle shell (Fig. 10).

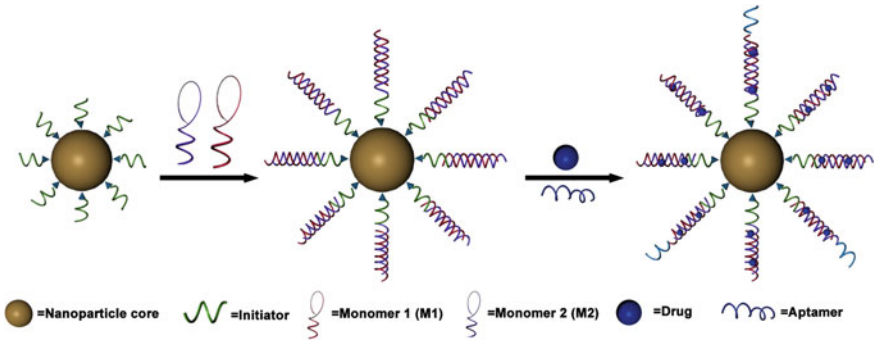

Fig. 10 Schematic representation of multimodal SNAs. Adapted with permission from Zheng et al. [108]. Copyright 2013

The monomer DNA sequences were designed to carry fluorophores for fluorescence imaging and targeting sequences for cell-specific recognition. One of the monomer DNA sequences contained an embedded aptamer AS1411, which forms a stable G-quadruplex structure that specifically targets nucleolin, a protein overexpressed in tumor cells [109]. AS1411 has been tested in phase II clinical trials for patients with relapsed or refractory acute myeloid leukemia and renal cell carcinoma [110]. In G-quadruplex form, AS1411 can bind 5, 10, 15, 20-tetrakis (4-N-methylpyridiniumyl)porphyrin (TMPyP4), a photodynamic therapy drug that is cytotoxic when exposed to light [111]. Hence, AS1411 enabled cell-specific targeting as well as drug loading capacity for these multimodal SNAs.

When nucleolin-expressing SKOV-3 ovarian epithelial adenocarcinoma cells and control, non-nucleolin-expressing HBE135 lung epithelial cells were incubated with FITC-labeled AS1411/MNP-SNAs and random, nontargeted MNP-SNAs, a significant fluorescence shift was found only with AS1411/MNP-SNAs in SKOV-3 cells, as assessed via flow cytometry. These data indicated that the binding capacity of the AS1411 aptamer remained intact after conjugation to the MNP-SNAs. Additionally, no significant fluorescence change was detected between the random MNP-SNAs and the AS1411/MNP-SNAs in HBE135 cells, indicating the specificity of the AS1411/MNP-SNAs for nucleolin.

Furthermore, a cytotoxicity assay was performed that compared TMPyP4 only to TMPyP4 bound on AS1411/MNP-SNAs (TMPyP4/AS1411/MNP-SNAs) in SKOV-3 and HBE135 cells. Cell death was induced by laser irradiation after treating with TMPyP4 only or TMPyP4/AS1411/MNP-SNAs for 10 min and assessed via flow cytometry monitoring of propidium iodide (PI)-labeled dead cells. The phototoxicity of the TMPyP4/AS1411/MNP-SNAs was significantly higher than TMPyP4 only in nucleolin-expressing SKOV-3 cells (IC_{50} of TMPyP4/AS1411/MNP-SNAs $\sim$0.15 μM vs. IC_{50} of TMPyP4 only $\sim$0.4 μM). Additionally, in non-nucleolin-expressing HBE135 cells, TMPyP4/AS1411/MNP-SNAs induced phototoxicity was significantly less than TMPyP4 only (IC_{50} of TMPyP4/AS1411/MNP-SNAs $\gg$3 μM vs. IC_{50} of TMPyP4 only $\sim$1.5 μM). These results indicated

that TMPyP4/AS1411/MNP-SNAs enabled cell-specific drug entry and acted as cytotoxic agents to nucleolin-expressing cancer cells, while protecting non-nucleolin-expressing control cells relative to TMPyP4 alone.

Thus, TMPyP4/AS1411/MNP-SNAs were shown to be a promising, multifunctional construct, with the ability to target cancer cells specifically, act as cytotoxic payloads to cancer cells, and be fluorescently imaged. Given the tunable nature of the monomer DNA sequences, these self-assembled, multimodal SNA conjugates are adaptable and could potentially be expanded as a therapeutic platform for cancer.

5 Future Outlook

Spherical nucleic acids (SNAs) represent a model platform for oligonucleotide-based therapeutics. These novel materials enter cells in high quantities without the use of transfection agents and can be utilized to regulate gene expression without eliciting an immune response. They are also resistant to nuclease degradation and can be formulated as multifunctional materials when the nucleic acids on their surface are conjugated to entities such as small molecules, drugs, or antibodies. While it is advantageous that these materials enter almost every known cell line and can cross the blood–brain and blood–tumor barriers as well as the epidermis, their use does not come without its own challenges. The nonspecific uptake of SNAs by virtually all cells must be addressed in the context of systemic delivery, and the coupling of SNAs to targeting moieties, such as antibodies, are being explored to increase their specificity for certain cell types. While their nonspecific uptake necessitates thoughtful target selection for systemic applications, SNAs are ideal candidates for local administration. The challenges for this class of therapeutics, going forward, will be picking appropriate genetic targets and diseases to treat. The fact that the oligonucleotide sequence can be tuned to specifically target a disease-causing mRNA sequence, while sparing healthy mRNA sequences, has tremendous potential for increasing the therapeutic precision and minimizing off-target effects. The customizable nature of the oligonucleotides becomes even more important when one considers that the genetic basis of many diseases is constantly changing and that diseases present themselves differently in each patient. SNAs may allow for on-demand, personalized, or individualized therapeutic options to combat ever-evolving microorganisms and cancer diversity.

References

1. Burnett JC, Rossi JJ, Tiemann K (2011) Current progress of siRNA/shRNA therapeutics in clinical trials. Biotechnol J 6(9):1130–1146
2. Stegh AH (2013) Toward personalized cancer nanomedicine—past, present, and future. Integr Biol 5(1):48–65
3. Burnett JC, Rossi JJ (2012) RNA-based therapeutics: current progress and future prospects. Chem Biol 19(1):60–71

4. Davidson BL, McCray PB (2011) Current prospects for RNA interference-based therapies. Nat Rev Genet 12(5):329–340
5. Kanasty R, Dorkin JR, Vegas A, Anderson D (2013) Delivery materials for siRNA therapeutics. Nat Mater 12(11):967–977
6. Kim DH, Rossi JJ (2007) Strategies for silencing human disease using RNA interference. Nat Rev Genet 8(3):173–184
7. Carthew RW, Sontheimer EJ (2009) Origins and mechanisms of miRNAs and siRNAs. Cell 136(4):642–655
8. Bennett CF, Swayze EE (2010) RNA targeting therapeutics: molecular mechanisms of antisense oligonucleotides as a therapeutic platform. Annu Rev Pharmacol Toxicol 50:259–293
9. Magen I, Hornstein E (2014) Oligonucleotide-based therapy for neurodegenerative diseases. Brain Res 1584:116–128
10. Cerritelli SM, Crouch RJ (2009) Ribonuclease H: the enzymes in eukaryotes. FEBS J 276 (6):1494–1505
11. Fire A, Xu S, Montgomery MK, Kostas SA, Driver SE, Mello CC (1998) Potent and specific genetic interference by double-stranded RNA in Caenorhabditis elegans. Nature 391 (6669):806–811
12. Castanotto D, Rossi JJ (2009) The promises and pitfalls of RNA-interference-based therapeutics. Nature 457(7228):426–433
13. Elbashir SM, Harborth J, Lendeckel W, Yalcin A, Weber K, Tuschl T (2001) Duplexes of 21-nucleotide RNAs mediate RNA interference in cultured mammalian cells. Nature 411 (6836):494–498
14. Hannon GJ, Rossi JJ (2004) Unlocking the potential of the human genome with RNA interference. Nature 431(7006):371–378
15. Novina CD, Sharp PA (2004) The RNAi revolution. Nature 430(6996):161–164
16. Hannon GJ (2002) RNA interference. Nature 418(6894):244–251
17. McManus MT, Sharp PA (2002) Gene silencing in mammals by small interfering RNAs. Nat Rev Genet 3(10):737–747
18. Zamore PD, Tuschl T, Sharp PA, Bartel DP (2000) RNAi: double-stranded RNA directs the ATP-dependent cleavage of mRNA at 21 to 23 nucleotide intervals. Cell 101(1):25–33
19. Bartlett DW, Davis ME (2007) Effect of siRNA nuclease stability on the in vitro and in vivo kinetics of siRNA-mediated gene silencing. Biotechnol Bioeng 97(4):909–921
20. Fabian MR, Sonenberg N, Filipowicz W (2010) Regulation of mRNA translation and stability by microRNAs. Annu Rev Biochem 79:351–379
21. Kanasty RL, Whitehead KA, Vegas AJ, Anderson DG (2012) Action and reaction: the biological response to siRNA and Its delivery vehicles. Mol Ther 20(3):513–524
22. Schroeder A, Levins CG, Cortez C, Langer R, Anderson DG (2010) Lipid-based nanotherapeutics for siRNA delivery. J Intern Med 267(1):9–21
23. Whitehead KA, Langer R, Anderson DG (2010) Knocking down barriers: advances in siRNA delivery. Nat Rev Drug Discov 9(5):412
24. Fichter KM, Ingle NP, McLendon PM, Reineke TM (2013) Polymeric nucleic acid vehicles exploit active interorganelle trafficking mechanisms. ACS Nano 7(1):347–364
25. Nelson CE, Kintzing JR, Hanna A, Shannon JM, Gupta MK, Duvall CL (2013) Balancing cationic and hydrophobic content of PEGylated siRNA polyplexes enhances endosome escape, stability, blood circulation time, and bioactivity in vivo. ACS Nano 7(10):8870–8880
26. Patil ML, Zhang M, Taratula O, Garbuzenko OB, He H, Minko T (2009) Internally cationic polyamidoamine PAMAM-OH dendrimers for siRNA delivery: effect of the degree of quaternization and cancer targeting. Biomacromolecules 10(2):258–266
27. Alabi CA, Love KT, Sahay G, Yin H, Luly KM, Langer R, Anderson DG (2013) Multiparametric approach for the evaluation of lipid nanoparticles for siRNA delivery. Proc Natl Acad Sci USA 110(32):12881–12886

28. Rungta RL, Choi HB, Lin PJC, Ko RWY, Ashby D, Nair J, Manoharan M, Cullis PR, MacVicar BA (2013) Lipid nanoparticle delivery of siRNA to silence neuronal gene expression in the brain. Mol Ther Nucleic Acids 2:e136
29. Nayerossadat N, Maedeh T, Ali PA (2012) Viral and nonviral delivery systems for gene delivery. Adv Biomed Res 1(2):14
30. Bharali DJ, Klejbor I, Stachowiak EK, Dutta P, Roy I, Kaur N, Bergey EJ, Prasad PN, Stachowiak MK (2005) Organically modified silica nanoparticles: a nonviral vector for in vivo gene delivery and expression in the brain. Proc Natl Acad Sci USA 102 (32):11539–11544
31. Giljohann DA, Seferos DS, Daniel WL, Massich MD, Patel PC, Mirkin CA (2010) Gold nanoparticles for biology and medicine. Angew Chem Int Ed 49(19):3280–3294
32. Kneuer C, Sameti M, Bakowsky U, Schiestel T, Schirra H, Schmidt H, Lehr C-M (2000) A nonviral DNA delivery system based on surface modified silica-nanoparticles can efficiently transfect cells in vitro. Bioconjug Chem 11(6):926–932
33. Cutler JI, Auyeung E, Mirkin CA (2012) Spherical nucleic acids. J Am Chem Soc 134 (3):1376–1391
34. Mirkin CA, Letsinger RL, Mucic RC, Storhoff JJ (1996) A DNA-based method for rationally assembling nanoparticles into macroscopic materials. Nature 382(15):607–609
35. Giljohann DA, Seferos DS, Patel PC, Millstone JE, Rosi NL, Mirkin CA (2007) Oligonucleotide loading determines cellular uptake of DNA-modified gold nanoparticles. Nano Lett 7(12):3818–3821
36. Choi CHJ, Hao L, Narayan SP, Auyeung E, Mirkin CA (2013) Mechanism for the endocytosis of spherical nucleic acid nanoparticle conjugates. Proc Natl Acad Sci USA 110 (19):7625–7630
37. Patel PC, Giljohann DA, Daniel WL, Zheng D, Prigodich AE, Mirkin CA (2010) Scavenger receptors mediate cellular uptake of polyvalent oligonucleotide-functionalized gold nanoparticles. Bioconjug Chem 21(12):2250–2256
38. Massich MD, Giljohann DA, Seferos DS, Ludlow LE, Horvath CM, Mirkin CA (2009) Regulating immune response using polyvalent nucleic acid—gold nanoparticle conjugates. Mol Biopharm 6(6):1934–1940
39. Zheng D, Giljohann DA, Chen DL, Massich MD, Wang XQ, Iordanov H, Mirkin CA, Paller AS (2012) Topical delivery of siRNA-based spherical nucleic acid nanoparticle conjugates for gene regulation. Proc Natl Acad Sci USA 109(30):11975–11980
40. Barnaby SN, Lee A, Mirkin CA (2014) Probing the inherent stability of siRNA immobilized on nanoparticle constructs. Proc Natl Acad Sci USA 111(27):9739–9744
41. Giljohann DA, Seferos DS, Prigodich AE, Patel PC, Mirkin CA (2009) Gene regulation with polyvalent siRNA—nanoparticle conjugates. J Am Chem Soc 131(6):2072–2073
42. Rosi NL, Giljohann DA, Thaxton CS, Lytton-Jean AKR, Han MS, Mirkin CA (2006) Oligonucleotide-modified gold nanoparticles for intracellular gene regulation. Science 312 (5776):1027–1030
43. Seferos DS, Prigodich AE, Giljohann DA, Patel PC, Mirkin CA (2009) Polyvalent DNA nanoparticle conjugates stabilize nucleic acids. Nano Lett 9(1):308–311
44. Hao L, Patel PC, Alhasan AH, Giljohann DA, Mirkin CA (2011) Nucleic acid-gold nanoparticle conjugates as mimics of microRNA. Small 7(22):3158–3162
45. Jensen SA, Day ES, Ko CH, Hurley LA, Luciano JP, Kouri FM, Merkel TJ, Luthi AJ, Patel PC, Cutler JI, Daniel WL, Scott AW, Rotz MW, Meade TJ, Giljohann DA, Mirkin CA, Stegh AH (2013) Spherical nucleic acid nanoparticle conjugates as an RNAi-based therapy for glioblastoma. Sci Transl Med 5(209):209ra152
46. Lee J-S, Lytton-Jean AKR, Hurst SJ, Mirkin CA (2007) Silver nanoparticle—oligonucleotide conjugates based on DNA with triple cyclic disulfide moieties. Nano Lett 7(7):2112–2115
47. Cutler JI, Zheng D, Xu X, Giljohann DA, Mirkin CA (2010) Polyvalent oligonucleotide iron oxide nanoparticle “click” conjugates. Nano Lett 10(4):1477–1480

48. Zhang C, Macfarlane RJ, Young KL, Choi CHJ, Hao L, Auyeung E, Liu G, Zhou X, Mirkin CA (2013) A general approach to DNA-programmable atom equivalents. Nat Mater 12 (8):741–746
49. Mitchell GP, Mirkin CA, Letsinger RL (1999) Programmed assembly of DNA functionalized quantum dots. J Am Chem Soc 121(35):8122–8123
50. Young KL, Scott AW, Hao L, Mirkin SE, Liu G, Mirkin CA (2012) Hollow spherical nucleic acids for intracellular gene regulation based upon biocompatible silica shells. Nano Lett 12 (7):3867–3871
51. Banga RJ, Chernyak N, Narayan SP, Nguyen ST, Mirkin CA (2014) Liposomal spherical nucleic acids. J Am Chem Soc 136(28):9866–9869
52. Calabrese CM, Merkel TJ, Briley WE, Randeria PS, Narayan SP, Rouge JL, Walker DA, Scott AW, Mirkin CA (2015) Biocompatible infinite-coordination-polymer-nanoparticle—nucleic-acid conjugates for antisense gene regulation Angew Chem Int Ed 54(2):476−480
53. Cutler JI, Zhang K, Zheng D, Auyeung E, Prigodich AE, Mirkin CA (2011) Polyvalent nucleic acid nanostructures. J Am Chem Soc 133(24):9254–9257
54. Morris W, Briley WE, Auyeung E, Cabezas MD, Mirkin CA (2014) Nucleic acid-metal organic framework (MOF) nanoparticle conjugates. J Am Chem Soc 136(20):7261–7264
55. Alemdaroglu FE, Alemdaroglu NC, Langguth P, Herrmann A (2008) DNA block copolymer micelles—a combinatorial tool for cancer nanotechnology. Adv Mater 20(5):899–902
56. Li Z, Zhang Y, Fullhart P, Mirkin CA (2004) Reversible and chemically programmable micelle assembly with DNA block-copolymer amphiphiles. Nano Lett 4(6):1055–1058
57. Rouge JL, Hao L, Wu XA, Briley WE, Mirkin CA (2014) Spherical nucleic acids as a divergent platform for synthesizing RNA-nanoparticle conjugates through enzymatic ligation. ACS Nano 8(9):8837–8843
58. Alexis F, Pridgen E, Molnar LK, Farokhzad OC (2008) Factors affecting the clearance and biodistribution of polymeric nanoparticles. Mol Pharm 5(4):505–515
59. Kommareddy S, Amiji M (2007) Biodistribution and pharmacokinetic analysis of long-circulating thiolated gelatin nanoparticles following systemic administration in breast cancer-bearing mice. J Pharm Sci 96(2):397–407
60. Zhang K, Hao L, Hurst SJ, Mirkin CA (2012) Antibody-linked spherical nucleic acids for cellular targeting. J Am Chem Soc 134(40):16488–16491
61. Nanba D, Toki F, Barrandon Y, Higashiyama S (2013) Recent advances in the epidermal growth factor receptor/ligand system biology on skin homeostasis and keratinocyte stem cell regulation. J Dermatol Sci 72(2):81–86
62. Krex D, Klink B, Hartmann C, von Deimling A, Pietsch T, Simon M, Sabel M, Steinbach JP, Heese O, Reifenberger G, Weller M, Schackert G, Network ftGG (2007) Long-term survival with glioblastoma multiforme. Brain 130(10):2596–2606
63. Pardridge WM (2012) Drug transport across the blood-brain barrier. J Cereb Blood Flow Metab 32(11):1959–1972
64. Goti D, Hrzenjak A, Levak-Frank S, Frank S, Van Der Westhuyzen DR, Malle E, Sattler W (2001) Scavenger receptor class B, type I is expressed in porcine brain capillary endothelial cells and contributes to selective uptake of HDL-associated vitamin E. J Neurochem 76 (2):498–508
65. Mackic JB, Stins M, McComb JG, Calero M, Ghiso J, Kim KS, Yan SD, Stern D, Schmidt AM, Frangione B, Zlokovic BV (1998) Human blood-brain barrier receptors for Alzheimer's amyloid-beta 1–40. Asymmetrical binding, endocytosis, and transcytosis at the apical side of brain microvascular endothelial cell monolayer. J Clin Invest 102(4):734–743
66. Stegh AH, Brennan C, Mahoney JA, Forloney KL, Jenq HT, Luciano JP, Protopopov A, Chin L, DePinho RA (2010) Glioma oncoprotein Bcl2L12 inhibits the p53 tumor suppressor. Genes Dev 24(19):2194–2204
67. Stegh AH, Chin L, Louis DN, DePinho RA (2008) What drives intense apoptosis resistance and propensity for necrosis in glioblastoma? A role for Bcl2L12 as a multifunctional cell death regulator. Cell Cycle 7(18):2833–2839

68. Stegh AH, DePinho RA (2011) Beyond effector caspase inhibition Bcl2L12 neutralizes p53 signaling in glioblastoma. Cell Cycle 10(1):33–38
69. Stegh AH, Kesari S, Mahoney JE, Jenq HT, Forloney KL, Protopopov A, Louis DN, Chin L, DePinho RA (2008) Bcl2L12-mediated inhibition of effector caspase-3 and caspase-7 via distinct mechanisms in glioblastoma. Proc Natl Acad Sci USA 105(31):10703–10708
70. Stegh AH, Kim H, Bachoo RM, Forloney KL, Zhang J, Schulze H, Park K, Hannon GJ, Yuan J, Louis DN, DePinho RA, Chin L (2007) Bcl2L12 inhibits post-mitochondrial apoptosis signaling in glioblastoma. Genes Dev 21(1):98–111
71. Boveri M, Berezowski V, Price A, Slupek S, Lenfant A-M, Benaud C, Hartung T, Cecchelli R, Prieto P, Dehouck M-P (2005) Induction of blood-brain barrier properties in cultured brain capillary endothelial cells: comparison between primary glial cells and C6 cell line. Glia 51 (3):187–198
72. Cecchelli R, Dehouck B, Descamps L, Fenart L, Buée-Scherrer V, Duhem C, Lundquist S, Rentfel M, Torpier G, Dehouck MP (1999) In vitro model for evaluating drug transport across the blood–brain barrier. Adv Drug Deliv Rev 36(2–3):165–178
73. Culot M, Lundquist S, Vanuxeem D, Nion S, Landry C, Delplace Y, Dehouck M-P, Berezowski V, Fenart L, Cecchelli R (2008) An in vitro blood-brain barrier model for high throughput (HTS) toxicological screening. Toxicol In Vitro 22(3):799–811
74. Petros RA, DeSimone JM (2010) Strategies in the design of nanoparticles for therapeutic applications. Nat Rev Drug Discov 9(8):615–627
75. Huse JT, Holland EC (2009) Yin and yang: cancer-implicated miRNAs that have it both ways. Cell Cycle 8(22):3611–3612
76. Iorio MV, Croce CM (2009) MicroRNAs in cancer: small molecules with a huge impact. J Clin Oncol 27(34):5848–5856
77. Iorio MV, Croce CM (2012) Causes and Consequences of MicroRNA dysregulation. Cancer J 18(3):215–222 210.1097/PPO.1090b1013e318250c318001
78. Kouri FM, Hurley LA, Day ES, Hua Y, Merkel TJ, Queisser MA, Peng C-Y, Ritner C, Hao L, Daniel WL, Zhang H, Sznajder JI, Chin L, Giljohann DA, Kessler JA, Peter ME, Mirkin CA, Stegh AH (2015) miR-182 integrates apoptosis, growth and differentiation programs in glioblastoma Genes and Development, in press
79. Cancer Genome Atlas Research N (2008) Comprehensive genomic characterization defines human glioblastoma genes and core pathways. Nature 455(7216):1061–1068
80. Geusens B, Sanders N, Prow T, Van Gele M, Lambert J (2009) Cutaneous short-interfering RNA therapy. Expert Opin Drug Deliv 6(12):1333–1349
81. Leachman SA, Hickerson RP, Schwartz ME, Bullough EE, Hutcherson SL, Boucher KM, Hansen CD, Eliason MJ, Srivatsa GS, Kornbrust DJ, Smith FJD, McLean WHI, Milstone LM, Kaspar RL (2009) First-in-human mutation-targeted siRNA Phase Ib trial of an inherited skin disorder. Mol Ther 18(2):442–446
82. Proksch E, Brandner JM, Jensen J-M (2008) The skin: an indispensable barrier. Exp Dematol 17(12):1063–1072
83. Roberts PJ, Der CJ (2007) Targeting the Raf-MEK-ERK mitogen-activated protein kinase cascade for the treatment of cancer. Oncogene 26(22):3291–3310
84. Zhu H, Acquaviva J, Ramachandran P, Boskovitz A, Woolfenden S, Pfannl R, Bronson RT, Chen JW, Weissleder R, Housman DE, Charest A (2009) Oncogenic EGFR signaling cooperates with loss of tumor suppressor gene functions in gliomagenesis. Proc Natl Acad Sci USA 106(8):2712–2716
85. Dickens S, Van den Berge S, Hendrickx B, Verdonck K, Luttun A, Vranckx JJ (2010) Nonviral transfection strategies for keratinocytes, fibroblasts, and endothelial progenitor cells for ex vivo gene transfer to skin wounds. Tissue Eng Part C Methods 16(6):1601–1608
86. Jamieson ER, Lippard SJ (1999) Structure, recognition, and processing of cisplatin—DNA adducts. Chem Rev 99(9):2467–2498

87. Rosenberg B, Vancamp L, Trosko JE, Mansour VH (1969) Platinum compounds: a new class of potent antitumour agents. Nature 222(5191):385–386
88. Lorusso D, Petrelli F, Coinu A, Raspagliesi F, Barni S (2014) A systematic review comparing cisplatin and carboplatin plus paclitaxel-based chemotherapy for recurrent or metastatic cervical cancer. Gynecol Oncol 133(1):117–123
89. Dhar S, Daniel WL, Giljohann DA, Mirkin CA, Lippard SJ (2009) Polyvalent oligonucleotide gold nanoparticle conjugates as delivery vehicles for platinum(IV) warheads. J Am Chem Soc 131(41):14652–14653
90. Wang D, Lippard SJ (2005) Cellular processing of platinum anticancer drugs. Nat Rev Drug Discov 4(4):307–320
91. Zhang X-Q, Xu X, Lam R, Giljohann D, Ho D, Mirkin CA (2011) Strategy for increasing drug solubility and efficacy through covalent attachment to polyvalent DNA–nanoparticle conjugates. ACS Nano 5(9):6962–6970
92. Dubois J (2006) Recent progress in the development of docetaxel and paclitaxel analogues. Expert Opin Ther Pat 16(11):1481–1496
93. Marupudi NI, Han JE, Li KW, Renard VM, Tyler BM, Brem H (2007) Paclitaxel: a review of adverse toxicities and novel delivery strategies. Expert Opin Drug Saf 6(5):609–621
94. Panchagnula R (1998) Pharmaceutical aspects of paclitaxel. Int J Pharm 172(1–2):1–15
95. Skwarczynski M, Hayashi Y, Kiso Y (2006) Paclitaxel prodrugs: toward smarter delivery of anticancer agents. J Med Chem 49(25):7253–7269
96. Gavrieli Y, Sherman Y, Ben-Sasson SA (1992) Identification of programmed cell death in situ via specific labeling of nuclear DNA fragmentation. J Cell Biol 119(3):493–501
97. Baselga J, Swain SM (2009) Novel anticancer targets: revisiting ERBB2 and discovering ERBB3. Nat Rev Cancer 9(7):463–475
98. Hynes NE, Lane HA (2005) ERBB receptors and cancer: the complexity of targeted inhibitors. Nat Rev Cancer 5(5):341–354
99. Hendriks BS, Opresko LK, Wiley HS, Lauffenburger D (2003) Quantitative analysis of HER2-mediated effects on HER2 and epidermal growth factor receptor endocytosis: distribution of homo- and heterodimers depends on relative HER2 levels. J Biol Chem 278 (26):23343–23351
100. Song Y, Xu X, MacRenaris KW, Zhang X-Q, Mirkin CA, Meade TJ (2009) Multimodal gadolinium-enriched DNA–gold nanoparticle conjugates for cellular imaging. Angew Chem Int Ed 121(48):9307–9311
101. Aime S, Cabella C, Colombatto S, Geninatti Crich S, Gianolio E, Maggioni F (2002) Insights into the use of paramagnetic Gd(III) complexes in MR-molecular imaging investigations. J Magn Reson Imaging 16(4):394–406
102. Bloembergen N (1956) Spin relaxation processes in a two-proton system. Phys Rev 104 (6):1542–1547
103. Bloembergen N (1957) Proton relaxation times in paramagnetic solutions. Chem Phys 27 (2):572–573
104. Bloembergen N, Morgan LO (1961) Proton relaxation times in paramagnetic solutions. effects of electron spin relaxation. Chem Phys 34(3):842–850
105. Solomon I (1955) Relaxation processes in a system of two Spins. Phys Rev 99(2):559–565
106. Solomon I, Bloembergen N (1956) Nuclear magnetic interactions in the HF molecule. Chem Phys 25(2):261–266
107. Merbach AE, Toth E (eds) (2001) The chemistry of contrast agents in medical magnetic resonance imaging. Wiley, New York
108. Zheng J, Zhu G, Li Y, Li C, You M, Chen T, Song E, Yang R, Tan W (2013) A spherical nucleic acid platform based on self-assembled DNA biopolymer for high-performance cancer therapy. ACS Nano 7(8):6545–6554

109. Girvan AC, Teng Y, Casson LK, Thomas SD, Juliger S, Ball MW, Klein JB, Pierce WM Jr, Barve SS, Bates PJ (2006) AGRO100 inhibits activation of nuclear factor-kappaB (NF-kappaB) by forming a complex with NF-kappaB essential modulator (NEMO) and nucleolin. Mol Cancer Ther 5(7):1790–1799
110. Hwang DW, Ko HY, Lee JH, Kang H, Ryu SH, Song IC, Lee DS, Kim S (2010) A nucleolin-targeted multimodal nanoparticle imaging probe for tracking cancer cells using an aptamer. J Nucl Med 51(1):98–105
111. Wang K, You M, Chen Y, Han D, Zhu Z, Huang J, Williams K, Yang CJ, Tan W (2011) Self-assembly of a bifunctional DNA carrier for drug delivery. Angew Chem Int Ed 50 (27):6098–6101

http://www.springer.com/978-3-319-16554-7

Nanotechnology-Based Precision Tools for the Detection and Treatment of Cancer

Mirkin, C.; Meade, Th.J.; Petrosko, S.H.; Stegh, A.H. (Eds.)

2015, X, 322 p. 100 illus., 96 illus. in color., Hardcover
ISBN: 978-3-319-16554-7